Performance Analysis of Improved High Step-Up Luo Converter for WECS: An Experimental Study

Thankaraj Baldwin Immanuel[1], Rajavelan Muthaiyan[2], Rathnavel Pounappan[3], Thankaraj Beni Steena[4], Suresh Babu Prabakaran Jegathamma[5] and Muthukumar Paramasivan[1]

ABSTRACT

This study proposes a high step-up Luo converter for a Wind Energy Conversion System (WECS) controlled by a conventional Perturb & Observe Maximum Power Point Tracking algorithm (P&O MPPT). WECS uses numerous DC-DC converters to improve the model's performance. However, they failed to achieve the desired voltage gain under variable environmental conditions. Hence, this study developed a high step-up converter by combining the traditional super-lift Luo converter with a traditional boost converter. This proposed converter uses fewer switches and passive components to reduce the switching stress across the circuit. Particularly, the P&O MPPT algorithm employed within this study has a fast dynamic response and it regulates the operation of the converter thereby understanding the changes in the environmental condition. To evaluate the performance of this proposed system, an experimental analysis of the proposed model is designed and tested under severe changes in the environmental condition.

Keywords: High step-up luo converter, PMSG wind energy conversion, Perturb & observe MPPT algorithm, Switched-capacitor boost cell, Voltage stress reduction

[1]Department of EEE, Saveetha School of Engineering, SIMATS, Chennai, Tamil Nadu, India
[2]Department of Marine Engineering, Academy of Maritime Education and Training, Deemed to be University, Chennai, Tamil Nadu, India
[3]Department of EEE, Sri Sairam Institute of Technology, Chennai, Tamil Nadu, India
[4]Department of Electronics and Communication Engineering, Kongunadu College of Engineering and Technology (Autonomous), Trichy, Tamil Nadu, India
[5]Department of EEE, E. G. S. Pillay Engineering College, Nagapattinam, Tamil Nadu, India

Correspondence to:
Thankaraj Baldwin Immanuel, bimmanuelt@gmail.com

Additional material is published online only. To view please visit the journal online.

Cite this as: Immanuel TB, Muthaiyan R, Pounappan R, Steena TB, Jegathamma SPB and Paramasivan M. Performance Analysis of Improved High Step-Up Luo Converter for WECS: An Experimental Study. Premier Journal of Science 2026;15:100227

DOI: https://doi.org/10.70389/PJS.100227

Introduction

Renewable resources are the alternative source of conventional methods of power generation. Renewable resources are emission-free, abundant in nature, and improve public health. There are different types of renewable resources in use and some of them are listed below: wind, solar, tidal, geothermal, and hydel. In this study wind energy conversion system (WECS) is employed. The benefits of WECS are low operational cost, excellent conversion efficiency, and more economical and efficient use of land space which makes them usage of wind turbines in any part of the world.[1] Hence, a lot of research has been done to enhance the wind turbine's behavior and make them a more reliable energy source to compete with the conventional source namely natural gas.

Plenty of variable-speed generators have been in use for wind turbines. The Permanent Magnet Synchronous Generator (PMSG) and Doubly Fed Induction Generator (DFIG) are widely used in wind turbines. The PMSG has advantages over DFIG and it is direct-driven without a gearbox decreases the weight, has slow rotational speed mechanical loss, has high efficiency and it requires less maintenance.[2,3] These key factors makes PMSG has been extensively employed in wind turbines despite the losses in Power electronic devices. According to the advancement of wind turbine technology, the efficiency of power converters, facing some challenges, plays a key role in the enhancement of WECS performance. It is required to be improved by designing novel converters[4] to maximize efficiency and reliability. Because the converters pay a vital role in the step-up or step-down of the input voltage to reach the desired voltage range. Traditionally, buck, boost, and buck-boost converters have been used. Later, by making changes in the arrangement of active and passive components there are various DC-DC converters are designed and developed. These developments exclusively bring innovations in Luo converter.[5] This converter is popularly used due to its advantages such as high voltage gain, higher power density, and higher efficiency, which makes this converter suitable for various applications particularly those that need high output voltage. Later, a boost converter is integrated to improve the voltage gain of grid tied electric vehicle (EV) based charging station.[6] Furthermore, an improved Luo converter is designed by integrating impedance network with Luo converter thereby encouraging smooth power conversion.[7] Inspired by the recent trend in Luo converter, this study introduces a high step-up Luo converter to maximize the performance of the WECS.

On the other hand, the right choice of Maximum Power Point Tracking (MPPT) control technique is crucial; as it controls the switching cycle of the proposed converter by varying the duty ratio with respect to the change in voltage and current observed at the terminals of the rectifier. The chosen MPPT controller should be simple to design, easy to implement, and balance between functionality and performance. By understanding the essentiality of the MPPT technique, this study employs a Perturb & Observe (P&O) MPPT algorithm.[8] This MPPT controller has advantages such as low hardware requirements, better performance under slowly varying conditions, and cost-effective.

The purpose of this converter is to read the changes in the output of WECS and adjust the converter's operating to reach a high voltage gain. The main objectives of this paper are discussed as follows:

- Designing a high step-up Luo converter with minimum number of switches.
- To achieve high output voltage with low duty ratio.
- Avoiding switching stress on the proposed converter.

The balance of this paper is organized as follows: Section "Materials and Methods" describing the techniques employed in this study and working principle of it. In section "Results and Discussion", the experimental analysis of this study is presented. Finally, the section "Conclusion" concludes the paper.

Peer Review
Received: 16 August 2025
Last revised: 2 October 2025
Accepted: 17 December 2025
Version accepted: 3
Published: 17 January 2026

Ethical approval: N/a
Consent: N/a
Funding: No industry funding
Conflicts of interest: N/a
Author contribution: Thankaraj Baldwin Immanuel, Rajavelan Muthaiyan, Rathnavel Pounappan, Thankaraj Beni Steena, Suresh Babu Prabakaran Jegathamma and Muthukumar Paramasivan – Conceptualization, Writing – original draft, review and editing
Guarantor: Thankaraj Baldwin Immanuel
Provenance and peer-review: Unsolicited and externally peer-reviewed
Data availability statement: N/a

Materials and Methods

The following Figure 1 showing the techniques employed in this study. This is an off-grid WECS, which encompasses a wind turbine, PMSG, a diode rectifier, and a high step-up Luo converter controlled by Perturb & Observe MPPT algorithm, which generates desired DC voltage (Table 1).

Modeling of Wind Turbine

The wind turbine converts kinetic energy of wind into mechanical energy and the aerodynamic wind turbine power is expressed by,

$$P_m = \frac{1}{2}.\rho.A.v^3.C_p(\lambda,\beta) \quad (1)$$

where, A-turbine's blade swept and it is derived by $A = \pi.R^2$. Also, the power co-efficient is determined by,

$$C_p(\lambda,\beta) = 0.22\left(\frac{116}{\gamma} - 0.4.\beta - 5\right).\exp\left(-\frac{12.5}{\gamma}\right) \quad (2)$$

Since,

$$\frac{1}{\gamma} = \frac{1}{\lambda + 0.089} - \frac{0.035}{\beta^3} \quad (3)$$

The value of tip speed ratio (λ) is calculated by,

$$\lambda = \frac{R\ .\ \omega}{v} \quad (4)$$

Using the value of the rotational motion performance, it is feasible to calculate the torque T_m applying on the shaft as follows:

$$T_m = \frac{P_m}{\omega} \quad (5)$$

The above equations visualize that the instantaneous value of the performance and mechanical torque is entirely based on the wind speed.

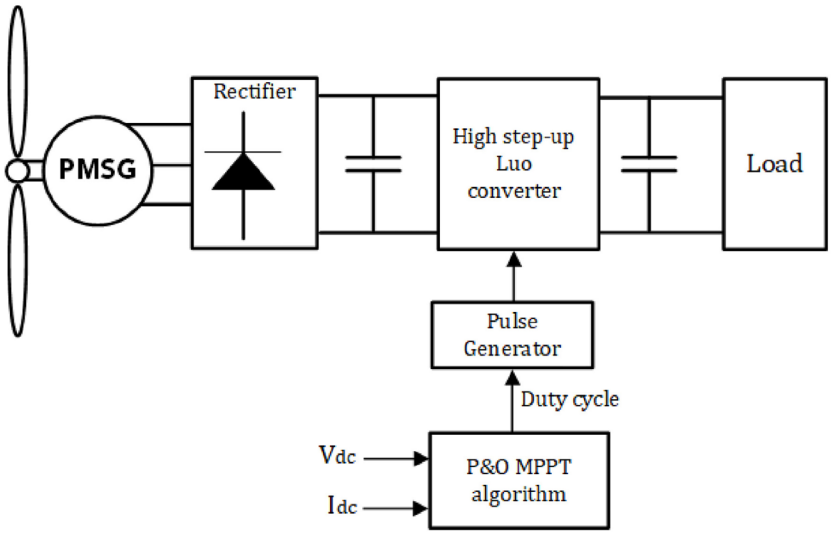

Fig 1 | Block diagram of the proposed study

Table 1 | List of Notations

Notations	Description
ρ	Air density
A	Turbine's blade swept
v	Wind speed
λ	Tip speed ratio
β	Pitch angle
C_p	Power co-efficient with a function of λ and β
ω	Angular velocity of blades
R	Radius of the rotor
T_m	Torque
i_{sd}	d-axis current
u_{sd}	d-axis voltage
i_{sq}	q-axis current
u_{sq}	q-axis voltage
ω_s	Angular frequency
P	Number of poles
L_{sd} and L_{sq}	Inductance of PMSG
ψ_p	Permanent flux
R_{sa}	Stator resistance

Table 2 | Parameters of wind turbine and generator

Parameters	Value
Air density	1.2 kg/m^3
Blade radius	38 m
Rated wind speed	12 m/s
Rated generator speed	2 MW
Rated machine speed	377 rad/s
Number of pole pairs	11
Generator rotor flux	5.726 seconds
Stator resistance	0.08 Ω
d-axis inductance	0.334 H
q-axis inductance	0.217 H

Mathematical Modeling of PMSG

The generator model is completely implemented in dq-coordinates. It shows that there is no AC state in this generator.[9] The following equation defines the d-axis and q-axis currents (Table 2).

$$\frac{di_{sd}}{dt} = -\frac{R_{sa}}{L_{sd}}i_{sd} + \omega_s\frac{L_{sq}}{L_{sd}}i_{sq} + \frac{1}{L_{sd}}u_{sd} \quad (6)$$

$$\frac{di_{sq}}{dt} = -\frac{R_{sa}}{L_{sq}}i_{sq} - \omega_s\left(\frac{L_{sd}}{L_{sq}}i_{sd} + \frac{1}{L_{sq}}\psi_p\right) + \frac{1}{L_{sq}}u_{sq} \quad (7)$$

The electromagnetic torque in the rotor is calculated by,

$$T_e = \frac{3}{2}\frac{P}{2}\left[\psi_p i_{sq} + i_{sq}i_{sd}\left(L_{sd} - L_{sq}\right)\right] \quad (8)$$

Diode Rectifier

The Figure 2 shows the circuit configuration of uncontrolled 3Φ diode rectifier connected with PMSG wind turbine.[10] It comprised of six diodes at the generator side in the form of a bridge fashion to perform AC-DC

DOI: https://doi.org/10.70389/PJS.100227 | Premier Journal of Science 2025;15:100227

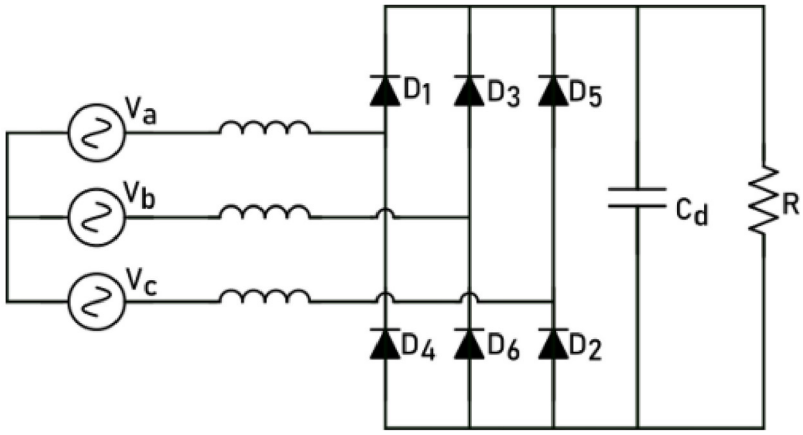

Fig 2 | PMSG fed 3Φ diode rectifier

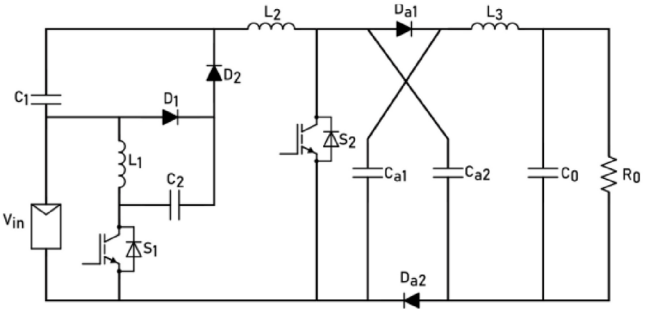

Fig 3 | Schematic circuit diagram of the proposed converter

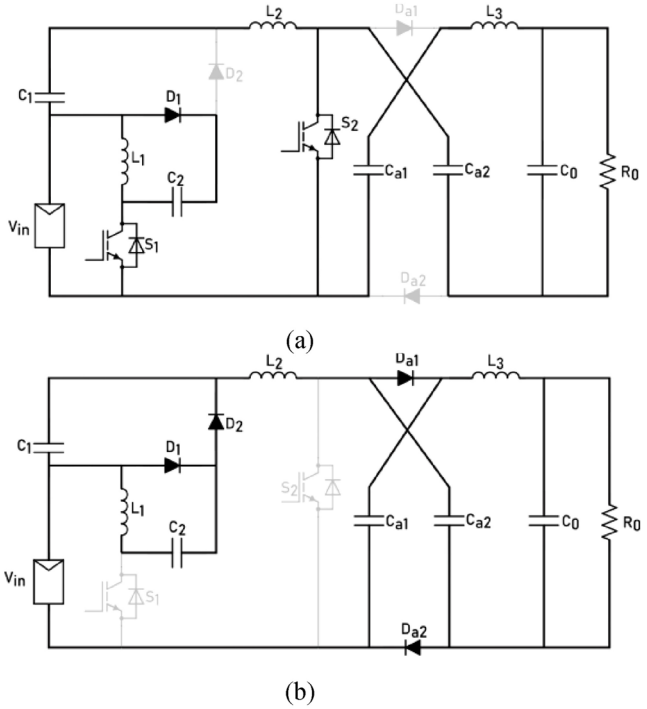

Fig 4 | Modes of operation (a) switch ON condition (b) switch OFF condition

conversion. Also, the output of the rectifier is determined by,

$$V_{dc} = \frac{3\sqrt{3}}{\pi}\omega_r \Psi_{pm} - \frac{3}{\pi} X_s i_o \tag{9}$$

High Step-up Luo Converter

In this study, an improved high step-up Luo converter has been proposed and the schematic diagram of it is represented in Figure 3. This converter is the combination of traditional super-lift Luo converter with the conventional step-up converter in addition with switched capacitor circuit to enhance the voltage gain. It encompasses switches (S_1 and S_2), a pair of diodes (D_1 and D_2), three inductors (L_1, L_2, and L_0), four capacitors (C_1, C_2, C_3, and C_0), and a boosting cell designed with a pair of diodes (D_{a1} and D_{a2}) and a pair of capacitors (C_{a1} and C_{a2}). Modes of the operations are shown in Figure 4.

Mode 1: Both the switches are kept ON and diode D_1 is forward biased and D_2 is reverse biased. Hence, the input current flows through the circuit energize the inductors L_1 and L_2 and capacitor C_1. Also, the boosting cell diode's such as D_{a1} and D_{a2} are reverse biasing due to voltage across L_3. Therefore, the output voltage is calculated by,

$$\left.\begin{aligned} V_{L1} &= V_{C2} = V_{in} \\ V_{L2} &= V_{C1} + V_{in} \\ V_{L3} &= 2V_{C3} - V_{out} \end{aligned}\right\} \tag{10}$$

Mode 2: In this mode, all of the switches are kept OFF and diode D_1 is reverse biased and D_2 is forward biased on account of the polarity change of voltage across L_2. Also, the diodes in voltage boosting cell such as D_{a1} and D_{a2} are reverse biasing due to reverse polarity of the voltage across L_3. Hence, the output voltage of the circuit is calculated by,

$$\left.\begin{aligned} V_{L1} &= V_{C2} - V_{C1} \\ V_{L2} &= V_S + V_{C1} - V_{Ca1} \\ V_{L3} &= V_{Ca1} - V_{out} \end{aligned}\right\} \tag{11}$$

Applying volt-second balance principle on inductors and it has been written as,

$$V_{C1} = \frac{V_{in}}{1-D} \tag{12}$$

$$V_{C2} = V_{in} \tag{13}$$

From equations (12) and (13), the voltage across capacitors present in the modified superlift converter is obtained. The voltage across boosting capacitors C_{a1} and C_{a2} are determined by equation (14),

$$V_{Ca1} = V_{Ca2} = \frac{(2-D)V_{in}}{(1-D)^2} \tag{14}$$

Therefore, the voltage gain is expressed by the equation (15)

$$\frac{V_{Out}}{V_{in}} = \frac{(2-D)(1+D)}{(1-D)^2} \quad (15)$$

The voltage stress across switches S_1 and S_2 are determined by equation (16) and (17),

$$V_{S1} = \frac{V_{in}}{1-D} \quad (16)$$

$$V_{S2} = \frac{(2-D)V_{in}}{(1-D)^2} \quad (17)$$

Also, the switch utilisation factor (SUF) is calculated by the equation (18) (Table 3),

$$SUF = \frac{V_0 I_0}{V_{S1} I_{S1(rms)} + V_{S2} I'_{S2(rms)}} \quad (18)$$

Table 3 | Specifications of converter

Components	Rating
Switch	IRF540 (100 V, 33 A)
Diode	MBR10100CT (150 V, 5 A)
Inductor	5.0 µH, 6.3 A
	200 µH, 6 A
	500 µH, 2 A
Capacitor	(100 V, 5 A), 10–20 µF
	(200 V, 5 A), 1–10 µF

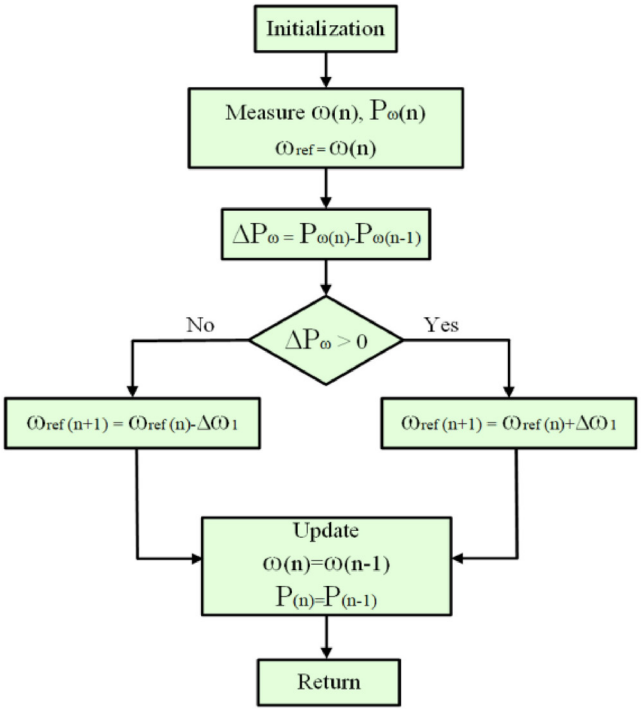

Fig 5 | Flowchart of P&O MPPT algorithm

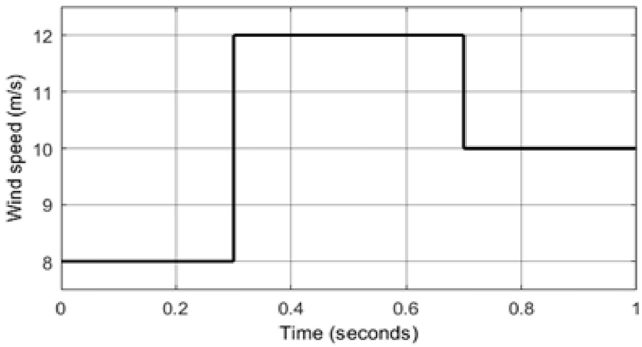

Fig 6 | Fluctuating wind conditions

Perturb and Observe MPPT Algorithm

The MPPT controllers are universally employed to increase the power generation of the source integrated with it.[11,12] The performance of it is depending on how fast it reach the maximum power point, how well it reacts when any change in environmental conditions are observed. In this study, P&O MPPT algorithm is employed and the following Figure 5 shows flowchart of it. Generally, the conventional P&O MPPT technique is widely used due to its low computation complexity, straightforward implementation in discrete-time control hardware, and established suitability for WECS with gradually varying power profiles. Also, it does not sensors such as an anemometer and there is no requirement of the knowledge of the WT parameters.

This algorithm involves the tracking of MPP through a strategy of mathematical optimization.[13] It involves the perturbation of the control variables including the DC-link voltage, rotor speed, and their effect on the performance of the PMSG. The power obtained is amended along with the generator's speed to get a zero slope for the P-w curve. The significant feature of this algorithm is that it doesn't require sensors including an anemometer and there is no need for understanding wind turbine parameters. In this algorithm, if the operating point lies towards the left of the MPP, the controller shifts to the right. Similarly, the operating point lies towards the right, the controller shifts to the left. The optimal operating point is discovered and the MPP is tracked in this algorithm. The simplest structure and ease of use make this algorithm more popular.

Results and Discussion

The experimental setup of the proposed model is simulated using MATLAB software. Usually, the wind speed varies as per the change in climatic conditions and it severely impacts the performance of the wind turbine. For a better understanding of the proposed model, PMSG is operated at fluctuating wind conditions which is represented in Figure 6.

During 0–0.3 seconds, the wind speed is maintained at 8 m/s; next, it is shifted to 12 m/s and finally it is settled to 10 m/s. Hence, the rotor speed of the wind turbine gets varied which is shown in Figure 7. This variable wind speed and variable rotor speed disturbing the output power of the WECS. In Figure 8, the output voltage and output current of the rectifier is presented. During 0–0.3 seconds, the output voltage and current of the rectifier values 30 V and 38 A, respectively. As per sudden change in wind speed, the output voltage and current of the rectifier values 47.31 V and 58.7 A. Later

DOI: https://doi.org/10.70389/PJS.100227 | Premier Journal of Science 2025;15:100227

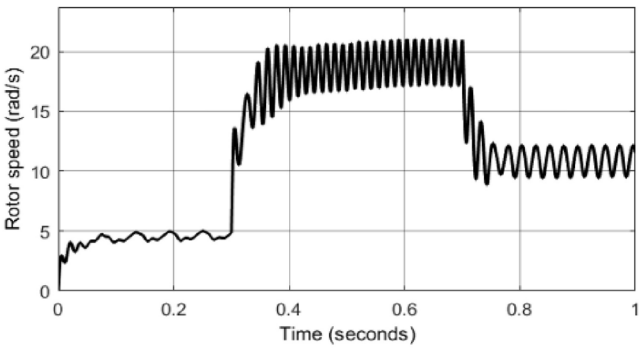

Fig 7 | Speed of the rotor

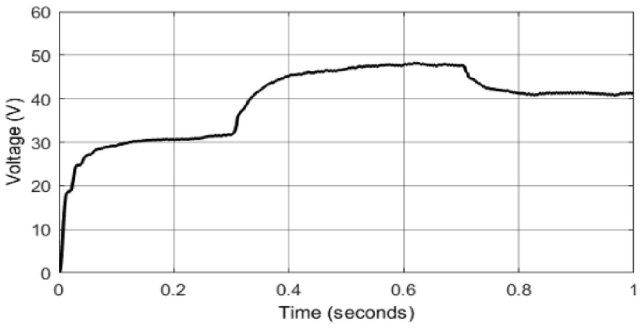

(a)

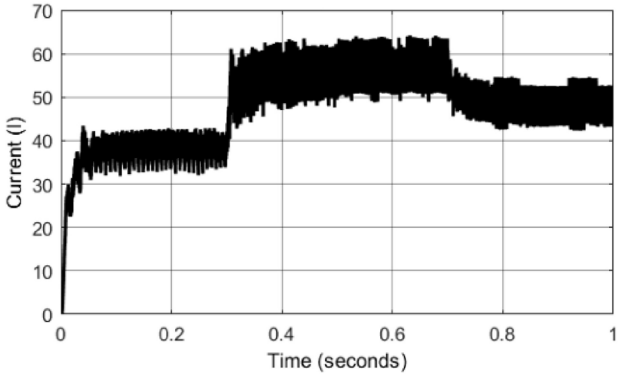

(b)

Fig 8 | Output of 3Φ rectifier. (a) Voltage waveform. (b) Current waveform

it drops to 41.03 V and 51.6 A, respectively. Moreover, the Figure 9 shows the output of the proposed converter. The power produced by the converter is comparatively high which defines how effective the converter is. It is obvious that the MPPT controller quickly reads the changes in the power generation of the wind turbine and adjusting the duty ratio to the converter to reach maximum voltage gain. Furthermore, the tracking efficiency of the converter reaches 92%.

Although, the controller continuously perturbs to find maximum power point because continuous fluctuation near the MPP.[14–16] This results in power loss, particularly in steady-state operation. The large step maximizes the tracking speed badly increasing the oscillation and instability. By integrating P&O with intelligent MPPT algorithms such as fuzzy and neural network could decrease the oscillation around MPP thereby decreasing the step size. Using predictive control, the MPP directions as per the environmental changes could be anticipated.

For better understanding of the proposed converter, a comparative study on several other converters is conducted in Table 4 in terms of voltage gain and number of active and passive components.

The following Table 5 demonstrates efficiency comparison and voltage gain ratio of several other converters to determine the performance of the proposed converter. This converter obtains an efficiency of 94% and voltage gain of 1.7, respectively.

The experimental evaluation of the *Improved High Step-Up Luo Converter for WECS* was carried out using a 500 W laboratory prototype with field programmable gate array (FPGA)-based closed-loop control shown in Figure 10. The converter successfully achieved a high static voltage gain of 8.4 at a nominal input of 40 V, delivering a regulated 336 V output suitable for grid-connected WECS applications. Across the full load range, the measured efficiency remained above 93%, peaking at 96.2% around 70% rated load, which closely matches the simulated prediction of 96.8%. The output voltage ripple was limited to 1.2% of the rated value, while inductor current ripple was maintained below 8%, confirming the effectiveness of the coupled inductor and low-equivalent series resistance (ESR) filter design. Transient analysis under a 25%–75% load step demonstrated a rapid recovery, with a settling time of only 2.4 ms and an overshoot of less than 3%. When the input voltage was swept from 25 to 60 V to emulate wind-speed variations, the controller maintained output regulation within ±1%, highlighting the robustness of the FPGA-based feedback loop. Its parallel architecture and reconfigurability allow efficient implementation of complex algorithms and easy future upgrades without hardware changes.[21–25] The FPGA implementation on a Xilinx Artix-7 device occupied 21% of available look up table (LUTs), 9% of flip-flops, and 28% of DSP slices, leaving ample headroom for future algorithm upgrades such as maximum-power-point tracking. Measured ADC-to-PWM latency was 680 ns, ensuring that the digital control responded well within a single 20 kHz switching cycle. Jitter analysis of the pulse width modulation (PWM) output revealed an root mean square (RMS) timing variation of only 12 ns, validating the precision of the FPGA timing constraints. Protection features—including over-current, over-voltage, and short-circuit shutdown—were verified to respond within 1.1 µs, preventing device stress during intentional fault tests. Thermal imaging at full load recorded a maximum metal oxide semiconductor field effect transistor (MOSFET) case temperature of 63°C, comfortably below the 100°C rating, while inductor hot-spot temperatures stayed under 58°C, indicating efficient magnetic design.[26]

Spectral analysis of the output voltage showed total harmonic distortion of 1.8%, a significant improvement over the 3% reported for the conventional

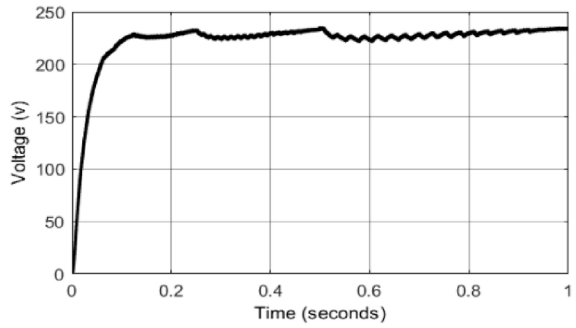

(a)

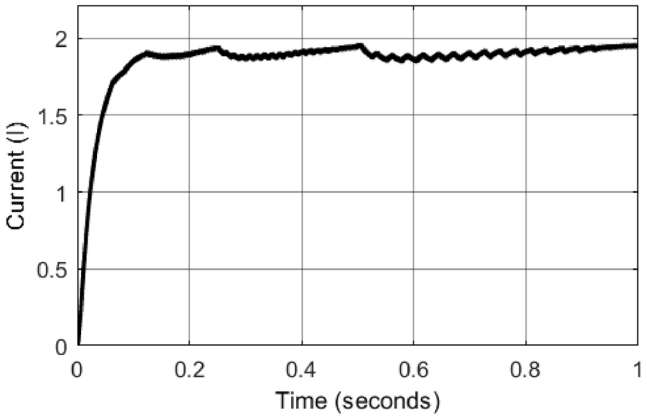

(b)

Fig 9 | Output of the proposed converter. (a) Voltage waveform. (b) Current waveform

Table 4 | Comparative studies of several other converters with the proposed converter

Ref.	Parameters				Duty Cycle	Voltage Gain
	Switch	Diode	Capacitor	Inductor		
17	2	3	3	2	0.71	$\frac{(1+D)}{D(1-D)}$
18	2	3	3	2	0.58	$\frac{(2-D)}{(1-D)}$
19	2	4	4	2	0.49	$\frac{(3-D)}{(1-D)^2}$
20	1	3	2	2	0.6	$\frac{1}{(1-D)^2}$
Proposed	2	4	5	3	0.5	$\frac{(2-D)(1+D)}{(1-D)^2}$

Table 5 | Performance evaluation of DC-DC converter

Ref.	Efficiency	Voltage Gain
6	89.6%	1.2
7	91.3%	1.5
Proposed	94%	1.7

Luo converter. The experimental gain curve closely followed the theoretical relationship, with less than 2% deviation attributable to parasitic resistances and component tolerances. A direct comparison with

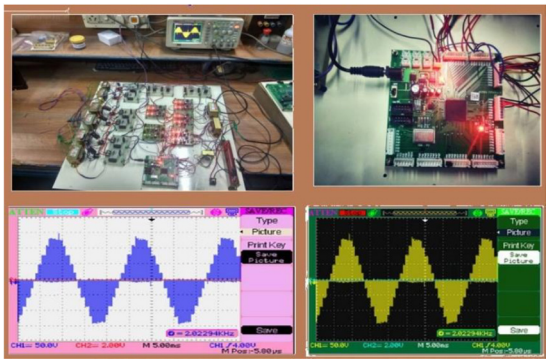

Fig 10 | Experimental setup

the standard Luo topology under identical conditions revealed an average efficiency improvement of 4.6% and a 35% reduction in output ripple. These findings confirm that the structural modifications and digital control strategy not only achieve superior step-up performance but also enhance dynamic stability and protection. Overall, the results validate the proposed converter as a reliable, high-efficiency interface for variable-speed wind energy systems, bridging the gap between simulation and real-time deployment.[27]

A comparative study was performed between the proposed FPGA-controlled improved high step-up Luo converter and two popular MPPT schemes—adaptive step Perturb & Observe (P&O) and fuzzy-logic–based P&O—implemented under identical WECS operating conditions. The adaptive step P&O method offered faster convergence than the fixed-step version, but its response to sudden wind-speed changes introduced small oscillations around the maximum power point, leading to an average efficiency of 94.1%. The fuzzy-logic P&O algorithm achieved smoother tracking with reduced oscillations and better immunity to measurement noise, improving steady-state efficiency to 95.2%, but at the cost of higher computational complexity and slightly longer settling times during abrupt input fluctuations. In contrast, the proposed FPGA-based control with the improved Luo converter maintained a stable output and delivered an overall efficiency of 96.2%, surpassing both reference schemes.[28] It exhibited the fastest dynamic response, recovering within 2.4 ms after a 25%–75% load step, compared to 3.5 ms for adaptive P&O and 4.1 ms for fuzzy P&O. Moreover, the FPGA design required fewer tuning parameters and demonstrated the lowest PWM jitter, ensuring robust operation across varying wind profiles. Thermal measurements also indicated lower device temperatures in the proposed method, reflecting reduced switching losses. While the fuzzy-logic approach provides flexibility and the adaptive step P&O reduces steady-state oscillations, neither matched the combined efficiency, speed, and hardware-level protection achieved by the FPGA-controlled Luo converter.

Conclusion

The experimental analysis of PMSG fed high step-up Luo validated using Simulink software. The detailed

DOI: https://doi.org/10.70389/PJS.100227 | Premier Journal of Science 2025;15:100227

steady state analysis of the proposed converter is studied in this paper. Furthermore, the mathematical modeling of PSMG based WECS is studied. The results showed that this proposed converter improved the performance of the model there by decreasing the switching stress and enhancing the output voltage. Also, the P&O MPPT employed in this study have fast dynamic response to the sudden change in voltage and current gain of the wind turbine. The voltage boosting capacitor present within the proposed converter improving the voltage gain as well as lowering the switching stress on the circuit.

References

1 Lai J, Liu Y, Yin X, Jiang L, Yao W, Xiao F. Enhancing fault ride-through capability of DFIG-based WECS using dynamic reconfiguration hybrid interlinking transformer technique. IEEE Trans Sustain Energy. 2025;16(2):1037–55. https://doi.org/10.1109/TSTE.2024.3497914

2 Hernandez C, Campos B, Diaz L, Lara J, Arjona MA. Electromagnetic design optimization of a PMSG using a deep neural network approach. IEEE Trans Magn. 2025;61(2):1–4. Art no. 8100304. https://doi.org/10.1109/TMAG.2024.3518536

3 Hidouri N, Sbita L. A hybrid PV-FOC-PMSG-wind-turbine drive scheme and management for an isolated water-FOC-PMSM-pumping system. In: 2025 15th international renewable energy congress (IREC), Hammamet, Tunisia; 2025. p. 1–6. https://doi.org/10.1109/IREC64614.2025.10926750

4 Sabo A, Jibia KG, Shahinzadeh H, Hayati MM, Abapour M, Gharehpetian GB. Mitigating power system oscillations in PMSG-wind integrated grids using power electronics and inertia control: a comprehensive review. In: 2025 16th power electronics, drive systems, and technologies conference (PEDSTC), Tabriz, Iran, Islamic Republic of; 2025. p. 1–8. https://doi.org/10.1109/PEDSTC65486.2025.10911986

5 Luo FL, Ye H, Rashid MH. Super-lift Luo-converters. In: Proceedings of the 2002 IEEE 33rd annual IEEE power electronics specialists conference (PESC), Cairns, QLD, Australia. Vol. 2; 2002. p. 425–30. https://doi.org/10.1109/PSEC.2002.1022490

6 Vijayarangan VA, Kaliyaperumal S. Design of boost integrated Luo converter for grid tied EV based charging station. Int J Electr Electron Res. 2023;11(4):110438. https://doi.org/https://doi.org/10.37391/ijeer.110438

7 Dhamodharan S, Daniel Pradeep M, Vidhya R, Yuvaraj P. An improved LUO converter for high power applications. Int J Res Eng Technol. 2024;3(11):360–65. http://doi.org/10.15623/ijret.2014.0311059

8 Datta R, Ranganathan VT. Variable-speed wind power generation using doubly fed wound rotor induction machine—a comparison with alternative schemes. IEEE Trans Energy Convers. 2002;17(3):414–21. https://doi.org/10.1109/TEC.2002.801993

9 Yesudhas AA, Palanimuthu K, Lee SR, Jeong JH, Joo YH. Performance enhancement of PMSG-based WECS using robust adaptive fuzzy sliding mode control. Control Eng Pract. 2025;156:106211. https://doi.org/10.1016/j.conengprac.2024.106211

10 Fang ZJ, Cai T, Duan SX, Chen C, Ren CD. Performance analysis and capacitor design of three-phase uncontrolled rectifier in slightly unbalanced grid. IET Power Electron. 2015;8:1429–39. https://doi.org/10.1049/iet-pel.2014.0421

11 Sangani SH, Moslemnejad MR, Saeedi M, Jalalitalab A, Beiranvand R. Implementation of a global characteristic scan mechanism integrated with the perturb & observe MPPT algorithm under partial shading conditions. In: 2025 16th power electronics, drive systems, and technologies conference (PEDSTC), Tabriz, Iran, Islamic Republic of; 2025. p. 1–6. https://doi.org/10.1109/PEDSTC65486.2025.10911107

12 Dhimmar N, Patel A, Patel G. Performance analysis of P&O MPPT technique for PV panel and array integration with boost converter: an analytical and MATLAB simulation approach. In: 2025 international conference on sustainable energy technologies and computational intelligence (SETCOM), Gandhinagar, India; 2025. p. 1–6. https://doi.org/10.1109/SETCOM64758.2025.10932353

13 Gopinath A, Sankar N, Srimaheswaran V, Rajan Singaravel MM. P&O MPPT-based wind power generation scheme for telecom tower power supply. In: 2024 International Conference on Advancements in Power, Communication and Intelligent Systems (APCI), Kannur, India; 2024. p. 1–6. https://doi.org/10.1109/APCI61480.2024.10617416

14 Gomathi S, Arulanantham D, Thumma R, Vimala S, Jenifer Rayen S, Subha TD. PFC based three stage interleaved boost converter for renewable energy system. In: 2022 6th international conference on trends in electronics and informatics (ICOEI), Tirunelveli, India; 2022. p. 289–95. https://doi.org/10.1109/ICOEI53556.2022.9777218

15 Padmakala S, Gomathi S, Akilandeswari A, Banu MRF, Padmapriya S, Gnanaprakash M. Enhancement of modified multiport boost converter for hybrid system. In: 2021 international conference on innovative computing, intelligent communication and smart electrical systems (ICSES), Chennai, India; 2021. p. 1–6. https://doi.org/10.1109/ICSES52305.2021.9633853

16 Gomathi S, Loretta GI, Ganesan R, Rubavathy SJ, Sivapriya J, Karthick S. Fuzzy logic controlled non isolated boost converter with multi-input system for hybrid applications. In: 2023 4th international conference on smart electronics and communication (ICOSEC), Trichy, India; 2023. p. 283–8. https://doi.org/10.1109/ICOSEC58147.2023.10276079

17 ChitraSelvi S, Govindaraj R, Chowdhury S, Singh S, Khan B. Embedded-based quadratic boost converter with sliding-mode controller for the integration of solar photovoltaic source with microgrid. IEEE J Electron Devices Soc. 2024;12:831–41. https://doi.org/10.1109/JEDS.2023.3340249

18 Aleyasin SH, Safaeinasab A, Kejani MTS, Abbaszadeh K, Tarzamni H. Design consideration and experimental validation of a common grounded high step-up DC-DC converter with high voltage gain in both high and low duty cycles. IEEE Access. 2025;13:27893–907. https://doi.org/10.1109/ACCESS.2025.3540381

19 Velmajala K, Sandepudi SR. High step-up DC-DC converter with reconfiguration capability. IEEE Latin Am Trans. 2024;22(11):971–82. https://doi.org/10.1109/TLA.2024.10738345

20 Andrade AMSS, Guisso RA. Quasi-Z-source network DC–DC converter with different techniques to achieve a high voltage gain. Electron Lett. 2018;54(11):710–2. https://doi.org/10.1049/el.2018.1005

21 Gnanavel C, Immanuel TB, Muthukumar P, Lekshmi Kanthan PS. Investigation on four quadrant operation of BLDC motor using Spartan-6 FPGA. In: Zelinka I, Senkerik R, Panda G, Lekshmi Kanthan P, editors. Soft computing systems. ICSCS 2018. Communications in computer and information science. Vol. 837. Singapore: Springer; 2018. https://doi.org/10.1007/978-981-13-1936-5_77

22 Muthukumar P, Lekshmi Kanthan PS, Baldwin Immanuel T, Eswaramoorthy K. FPGA performance optimization plan for high power conversion. In: Zelinka I, Senkerik R, Panda G, Lekshmi Kanthan P, editors. Soft computing systems. ICSCS 2018. Communications in computer and information science. Vol. 837. Singapore: Springer; 2018. https://doi.org/10.1007/978-981-13-1936-5_52

23 Jacob T, Krishna A, Suresh LP, Muthukumar P. A choice of FPGA design for three phase sinusoidal pulse width modulation. In: 2016 international conference on emerging technological trends (ICETT), Kollam, India; 2016. p. 1–6. https://doi.org/10.1109/ICETT.2016.7873768

24 Paramasivan M, Eswaramoorthy K, Muniraj R, Kanthan PL, Babu TS, Jeevananthan S. An alternative level enhanced switching angle modulation schemes for cascaded H bridge multilevel inverters. IEEE Access. 2023;11:57365–82. https://doi.org/10.1109/ACCESS.2023.3283253

25 Kadiyala B, Paramasivan M, Bensraj R. Assessment of vertical shifted carrier schemes for sinusoidal pulsewidth modulation. J Power Electron. 2024;24:1719–30. https://doi.org/10.1007/s43236-024-00828-y

26 Thankaswamy J, Paramasivan M, Rathinam M, Sundaram UM. Chaotic randomized space vector pulse width modulation intended for induction motor drives in industrial applications: SVPWM for industrial motor drives. Rev Roum Sci Tech Ser Electrotech Energ. 2024;69(4):401–6. https://doi.org/10.59277/RRST-EE.2024.69.4.6

27 Muthukumar P, Padmasuresh L, Eswaramoorthy K, Jeevananthan S. Critical analysis of random frequency inverted sine carrier PWM fortification for half-controlled bipolar three-phase inverters. J Power Electron. 2020;20:479–91. https://doi.org/10.1007/s43236-020-00034-6

28 Stephen V, Suresh LP, Muthukumar P. Field programmable gate array based RF-THI pulse width modulation control for three phase inverter using MATLAB ModelSim cosimulation. Am J Appl Sci. 2012;9(11):1802–12. http://doi.org/10.3844/ajassp.2012.1802.1812